Efficiency Enhancement in Organic Photovoltaic Cells: Consequences of Optimizing Series Resistance

By *Jonathan D. Servaites, Sina Yeganeh, Tobin J. Marks,** and *Mark A. Ratner**

Here, means to enhance power conversion efficiency (PCE or η) in bulk-heterojunction (BHJ) organic photovoltaic (OPV) cells by optimizing the series resistance (R_s)—also known as the cell internal resistance—are studied. It is shown that current state-of-the-art BHJ OPVs are approaching the limit for which efficiency can be improved via R_s reduction alone. This evaluation addresses OPVs based on a poly(3-hexylthiophene):6,6-phenyl C_{61}-butyric acid methyl ester (P3HT:PCBM) active layer, as well as future high-efficiency OPVs ($\eta > 10\%$). A diode-based modeling approach is used to assess changes in R_s. Given that typical published P3HT:PCBM test cells have relatively small areas ($\sim$0.1 cm^2), the analysis is extended to consider efficiency losses for larger area cells and shows that the transparent anode conductivity is then the dominant materials parameter affecting R_s efficiency losses. A model is developed that uses cell sizes and anode conductivities to predict current–voltage response as a function of resistive losses. The results show that the losses due to R_s remain minimal until relatively large cell areas (>0.1 cm^2) are employed. Finally, R_s effects on a projected high-efficiency OPV scenario are assessed, based on the goal of cell efficiencies >10%. Here, R_s optimization effects remain modest; however, there are now more pronounced losses due to cell size, and it is shown how these losses can be mitigated by using higher conductivity anodes.

1. Introduction

Organic photovoltaic (OPV) cells[1–5] offer the potential to change our energy landscape due to low production costs, mechanical flexibility, and the versatility of organic materials design.[6,7] However, while there have been significant gains in OPV cell power conversion efficiencies, they have not reached the level of conventional inorganic photovoltaics.[8,9] State-of-the-art bulk heterojunction (BHJ)[2,7,10] OPVs currently achieve cell efficiencies up to $\sim$6% under the standard solar spectrum, AM1.5G.[4,6,11–15] However, significant improvements are still needed, with efficiencies of 10% or greater generally regarded as necessary for widespread commercial viability.[4,16] Various useful approaches to BHJ OPV designs have been employed, such as using novel organic materials[4,11,17–22] or organic–inorganic hybrids[23,24] as active layer materials, incorporating designed interfacial layers at either electrode,[14,15,25] and employing tandem cells.[13] While these approaches offer significant advantages, loss mechanisms in OPVs still are not completely articulated. Establishing an improved understanding of these losses should provide research focus in increasing power conversion efficiencies to 10% and greater.

One of the key solar cell parameters affecting the cell power conversion efficiency (PCE or η) is the series resistance, or internal resistance, R_s. The series resistance represents the total resistance of the cell and is a composite of: 1) the active and interfacial layer resistances, 2) electrode resistances, and 3) the various contact and interconnect resistances.[26,27] It is known that R_s can have a pronounced effect on the solar cell fill factor (β_{FF}), which is defined as:[26–29]

$$\beta_{FF} = \frac{J_{\max} V_{\max}}{J_{sc} V_{oc}} \quad (1)$$

where $J_{\max}$ and $V_{\max}$ are the current density and voltage, respectively, at the maximum power output of the solar cell, J_{sc} is the cell short circuit current density, and V_{oc} is the cell open circuit voltage. The fill factor is one of three primary factors in determining η:[26–28]

$$\eta = \frac{\beta_{FF} J_{sc} V_{oc}}{P_{solar}} \quad (2)$$

where P_{solar} is the incident solar radiation. R_s is often the dominant parameter determining the fill factor (by altering the slope of the current density–voltage (J–V) curve near the V_{oc})[26] and is therefore of key importance for high-efficiency solar cells.

Organic semiconductors used in solar cells have mobilities typically several orders of magnitude lower than their inorganic

[*] Prof. T. J. Marks, Prof. M. A. Ratner, J. D. Servaites, S. Yeganeh
Departments of Chemistry and Materials Science and Engineering
Materials Research Center
and Argonne-Northwestern Solar Energy Research Center
Northwestern University
Evanston, IL 60208 (USA)
E-mail: t-marks@northwestern.edu; ratner@northwestern.edu

DOI: 10.1002/adfm.200901107

counterparts (e.g., silicon, gallium arsenide).[6,26] Therefore, active layer mobility enhancement and R_s reduction have been major OPV research focus areas in recent years. Previous studies have demonstrated significant reductions in OPV R_s values using new materials[30,31] or fabrication techniques[6,14,32] and concluded that the observed efficiency increases are largely due to R_s reduction. Thus, Li et al. demonstrated significant improvements in R_s and η for BHJ OPVs by optimizing film growth rates, showing that more slowly grown, phase-separated films benefit from improved molecular self-organization and, consequently, improved hole mobilities.[6] The benefits of self-organization from slow film growth rates have been characterized, as well as the morphological effects of different solvents and annealing rates.[6,33–36] However, despite the significant improvements in BHJ OPV mobilities, Li et al. reported maximum time-of-flight mobilities[6] on the order of only $10^{-4}\,cm^2\,V^{-1}\,s^{-1}$—several orders of magnitude less than those of typical inorganic solar cell and organic transistor materials.[26,37] Furthermore, the resistance of the active layer is proportional to the inverse of the mobility.[38] Therefore, the currently large differences in mobilities between organic and inorganic solar cell active layer materials raise the question of whether and to what degree OPV cell efficiencies suffer from large R_s values.

While previous authors have concluded that increases in active layer mobilities are correlated with lower R_s values and, ultimately, greater cell efficiencies,[6,14,30–32] there remains a need for a thorough, quantitative evaluation of the R_s–η relationship. To direct future efforts, it is important to understand how additional OPV R_s and mobility improvements will affect η. Previous studies provide useful guidance for modeling efficiency optimization, but their focus was primarily on energy level parameters for donor and acceptor materials.[2,39,40] A thorough analysis of OPV efficiency optimization based on series resistance considerations is also crucial, particularly given the attention it has received in OPV research. Providing such an optimization analysis should help guide future OPV materials development. We proceed here from an established relationship describing J–V behavior in solar cells and directly accounting for resistance (R_s) effects on cell performance:[26,27]

$$J = J_o\left[\exp\left(\frac{e(V - JR_s)}{nk_BT}\right) - 1\right] + \frac{V - JR_s}{R_p} - J_L \qquad (3)$$

where J_o is the reverse saturation current, e is the elementary charge, V is the cell voltage, J is the current density, n is the diode ideality factor, k_B is Boltzmann's constant, T is temperature, R_p is the equivalent circuit shunt, or parallel resistance, and J_L is the photocurrent generated by the cell before recombination losses. The application of Equation 3 to OPVs has been previously discussed.[41–44] Equation 3 stems from the original work of Shockley and co-workers to describe the ideal diode behavior of a p–n junction.[45,46] Later, Shockley, Read, and Hall modified this p-n junction analysis to account for deviations from ideal diode behavior (i.e., non-ideal p–n junctions having $n>1$).[47,48] OPVs exhibit the circuit characteristics expressed in Equation 3, and research is still in progress to understand the factors underlying J_o and n in OPVs. Extensions to Equation 3 have also been made to account for the effects of light intensity.[41,44,49] Other useful modeling approaches have also been suggested.[50–53] Our approach builds on Equation 3, which enables direct and quantitative evaluation of R_s effects on cell response.

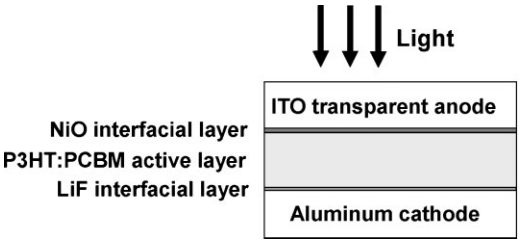

Figure 1. Diagram of a glass/ITO/NiO/P3HT:PCBM/LiF/Al bulk heterojunction OPV cell. The measured cell power conversion efficiency is 5.2%. See Ref. [14] for details on the cell preparation and characterization.

We report a comprehensive analysis of R_s effects on OPV power conversion efficiency through a combined experimental data-computational approach. We begin by studying a BHJ OPV cell design based on poly(3-hexylthiophene) and 6,6-phenyl C_{61}-butyric acid methyl ester (P3HT:PCBM) as the baseline. P3HT:PCBM systems have shown some of the largest reported single layer cell efficiencies for OPVs[4,6,14] and are therefore of interest when analyzing BHJ OPV efficiency losses. The design and fabrication details for these cells were recently reported.[14] Figure 1 shows the architecture of these cells. The devices have a nickel oxide (NiO) interfacial layer on the indium tin oxide (ITO) anode and a lithium fluoride (LiF) interfacial layer on the aluminum cathode, giving the overall cell structure glass/ITO/NiO/P3HT:PCBM/LiF/Al[14] (note that we refer to this cell design as the ''P3HT:PCBM test cell'' throughout this paper). To evaluate the effects of optimizing R_s, we use a least-squares fit to extract R_s, as well as the other parameters in Equation 3 (R_p, n, and J_o), from the previously reported current-voltage dark data.[14] Despite the relatively low mobilities of the organic active layer materials, this analysis will show that this P3HT:PCBM cell design is approaching the theoretical limit in R_s; further optimizing R_s (i.e., $R_s = 0$) would lead to an improvement in η of only $\sim 0.1\%$ (from 5.2% to 5.3%). Next, since the goal of OPV development is ultimately to move beyond systems in the 5% efficiency regime, we evaluate the effects of losses due to R_s for the important scenario of projected high-efficiency OPV cells (i.e., $\eta > 10\%$). Finally, noting that current laboratory-scale OPV cells reported in the literature typically have modest areas (e.g., $0.06\,cm^2$), we evaluate the effects of series resistance losses for larger area cells, finding that the anode resistance is the only remaining materials property that significantly effects a change in R_s for P3HT:PCBM cells, as well as for other OPVs with comparable R_s values. We conclude by using this analysis to offer a framework for investigating future OPV design strategies.

2. Results

2.1. Evaluation of Simulation Accuracy

Figure 2 shows a comparison of our simulated data and previously reported experimental data, using the standard solar spectrum

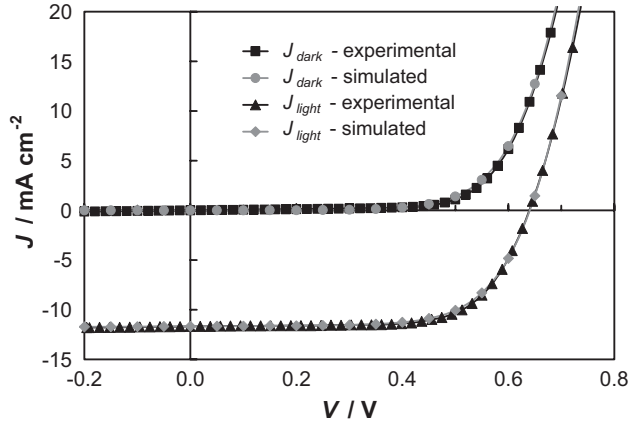

Figure 2. Experimental and simulated light and dark *J–V* curves from Equation 3 for a glass/ITO/NiO/P3HT:PCBM/LiF/Al test cell (depicted in Fig. 1 and discussed in Ref. [14]). The parameters for the simulated curves are given in Table 1. Note that this cell type is referred to as the ''P3HT:PCBM test cell'' throughout this contribution. The experimental data (from Ref. [14]) and the simulation curves closely overlap, giving $\eta = 5.2\%$.

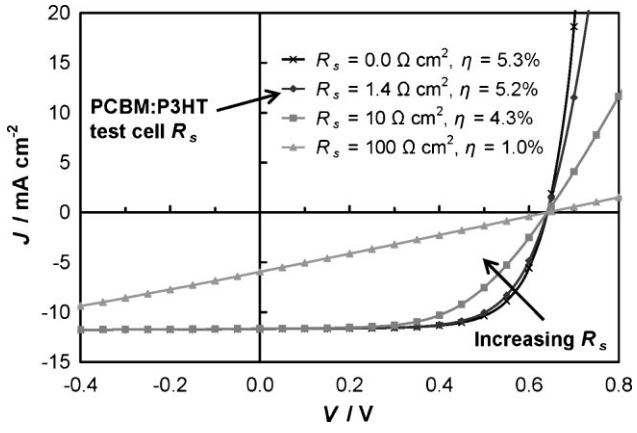

Figure 3. The effect of R_s variation on projected *J–V* characteristics for the P3HT:PCBM test cell. These data assume that R_s is the only parameter that changes; all other parameters in Equation 3 are held constant (i.e., J_L, R_p, n, and J_o). The parameters for these curves are given in Table 1. For the test cell, $R_s = 1.4\,\Omega$ cm^2, and $\eta = 5.2\%$. For a zero resistance cell (i.e., $R_s = 0$), η increases by only 0.1% to 5.3%. Large R_s values ($\sim 100\,\Omega$ cm^2) have significant effects on cell efficiency (e.g., an R_s of $100\,\Omega$ cm^2 reduces the cell efficiency to 1.0%).

(AM1.5G).[14] The simulated data are based on a least-squares fit to Equation 3 (details in Section 5). There is excellent agreement for both light and dark currents. Extracted fit parameters are summarized in Table 1. Previous work has addressed other modifications to Equation 3 to account for light intensity effects,[41,44] but these modifications are unnecessary here since the experimental *J–V* data indicate effective charge collection of the photocurrent.[54] Another approach for extracting R_s is often used by taking the slope of the *J–V* curve at high cell voltages (e.g., 2 V).[55] However, since organic semiconductor mobilities are often dependent on cell voltage,[56] it is preferable to extract R_s near actual operating voltages. Fitting Equation 3 enables this, and thus this approach should be a more accurate means of determining R_s.

2.2. R_s Effects on η, J_{sc}, and Fill Factor

Figure 3 shows simulations of how the cell *J–V* characteristics change with increasing R_s values. These curves are generated from Equation 3 and the parameters in Table 1, with R_s the only parameter being varied. The simulation shows how R_s impacts the key performance parameters: fill factor is significantly affected by increases in the P3HT:PCBM cell R_s, V_{oc} does not change, and J_{sc} only changes at very large R_s values (between 10 and $100\,\Omega$ cm^2). Figure 3 shows that completely eliminating R_s losses affords a very minor enhancement in η of ~0.1%—from 5.2% to 5.3%. Comparable experimental R_s effects on the cell *J–V* response of other BHJ OPVs have been reported, demonstrating the predictive value of this modeling approach in analyzing R_s effects. For example, Ma et al. showed how changes in annealing conditions led to improved active layer crystallinity and therefore reduced R_s values (due to increased mobilities of the more crystalline component materials).[11] The R_s variations for their experimental samples exhibit *J–V* response effects comparable to the calculated results in Figure 3. However, the lower limit of their R_s values was $\sim 10\,\Omega$ cm^2; the present computational method can address efficiency enhancements in the limit of $R_s \approx 0$—for example, to assess how further mobility enhancements would affect efficiency losses from cell resistance.

Figure 4 shows how η and fill factor are affected by R_s variations. Since the R_s value ($1.4\,\Omega$ cm^2) for the PCBM:P3HT test cell is at the

Table 1. Derived fit parameters R_s, R_p, n, and J_o for the P3HT:PCBM test cell in Figure 1.

R_s [Ω cm^2]	R_p [Ω cm^2]	n	J_o [A cm^{-2}]	J_L [A cm^{-2}]
1.4	3960 Ω cm^2	2.38	3.65×10^{-7}	0.0117

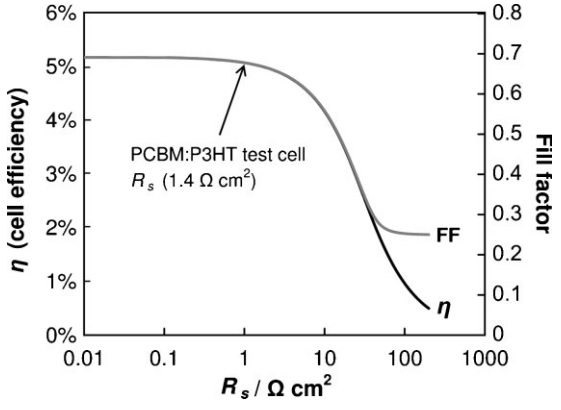

Figure 4. The projected effect of R_s on cell power conversion efficiency and fill factor (FF) for the P3HT:PCBM test cell. These data project how η and fill factor would change as the cell resistance changes, with all other cell parameters in Equation 3 held constant (i.e., J_L, R_p, n, and J_o). Note that the two curves are coincident until R_s approaches $\sim 50\,\Omega$ cm^2, at which point J_{sc} is also affected by R_s increases, thereby contributing to the efficiency losses.

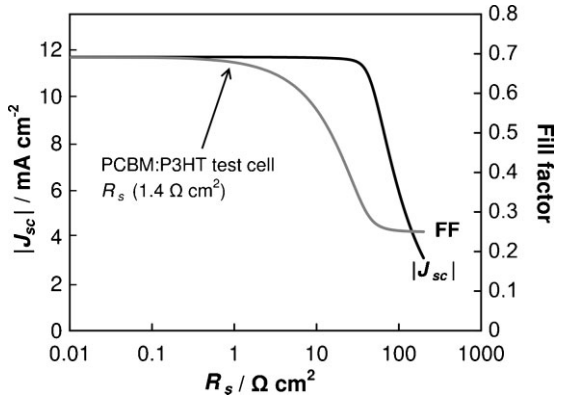

Figure 5. The projected effect of R_s on the cell short circuit current density (J_{sc}) and fill factor for the P3HT:PCBM test cell. These data project how J_{sc} and fill factor change if the cell resistance changes, with the other cell parameters in Equation 3 held constant (i.e., J_L, R_p, n, and J_o). The test cell R_s (1.4 Ω cm^2) is at the knee in the fill factor (FF) curve, but well beyond the knee in the J_{sc} curve.

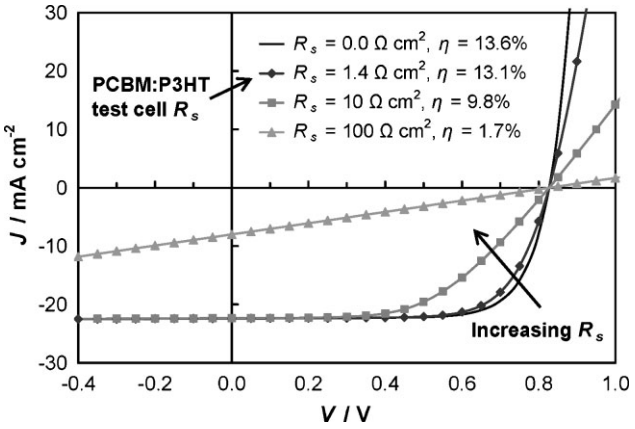

Figure 6. The effect of R_s variation on the J–V characteristics for a projected high-efficiency OPV cell, as outlined in Section 2.3. The parameters for these curves are given in Table 2. For R_s in the present P3HT:PCBM cell (1.4 Ω cm^2), this gives $\eta = 13.1\%$, compared with $\eta = 13.6\%$ for the zero R_s loss case. Note that the losses from R_s increases are significantly greater for the high-efficiency J–V curves than for the P3HT:PCBM test cell case (Fig. 3).

knee in both curves, further reductions in R_s afford only minor enhancements in cell performance, although moderate increases in R_s produce significant declines in both η and fill factor. Note that η and fill factor track each other almost exactly until R_s approaches ~50 Ω cm^2. At this point, losses in both fill factor and J_{sc} affect η, and fill factor and η curves diverge as shown in Figure 4. This divergence is due to effects on J_{sc} as R_s approaches ~50 Ω cm^2; the R_s–J_{sc} relationship is shown in Figure 5. For the present PCBM:P3HT cell design, there is a strong R_s–J_{sc} correlation only at high R_s values; R_s must increase by almost two orders of magnitude before there is a noticeable effect on J_{sc} (at which point J_{sc} declines rapidly with further R_s increases). The same fill factor data from Figure 4 are shown in Figure 5 for comparison, highlighting the fact that in the PCBM:P3HT test cell regime ($R_s \approx$ 1 Ω cm^2), fill factor is dramatically more sensitive to R_s than is J_{sc}. See Section 3 for a discussion of this analysis and the possibility of coupling between R_s and other parameters from Equations 2 and 3.

2.3. Evaluation of R_s Losses for a Projected High-Efficiency OPV Scenario

We evaluate here the effects of R_s losses for a scenario of high-efficiency OPV cells. To generate data for the high-efficiency case, we choose a model based upon a combination of the P3HT:PCBM test cell attributes and future target properties for OPVs.[15,20,57–59] These targets address the limitations of the P3HT:PCBM and other current OPV systems, which have been previously discussed.[2,39,40] The limitations reflect mismatches between donor and acceptor energy levels and the need for lower bandgap (~1.5 eV) materials. Note that the offset between the lowest unoccupied molecular orbitals of the donor ($LUMO_D$) and acceptor ($LUMO_A$) materials is critical. We assume here that the optimal case is a $LUMO_D/LUMO_A$ offset of 0.4 eV. With all other factors being equal, this offset would be a significant advance over current state-of-the-art OPV systems, and it appears to be realizable judging from recent experimental[22] and computational results.[39,60] Some materials are expected to require significantly larger $LUMO_D/LUMO_A$ offsets for efficient exciton dissociation (e.g., in the case of low dielectric constant environments or low carrier mobilities).[61–64] Our modeling here is based upon the expectation that, at low LUMO offsets, these exciton dissociation challenges will be overcome and that other materials and device characteristics will remain on par with the present P3HT:PCBM system (i.e., equivalent R_s, R_p, n, and external quantum efficiency (EQE) values). These energy level optimizations would allow for increased J_{sc} through increased light absorption (i.e., lower bandgap materials) and increased V_{oc} through better donor-acceptor energy level matching.[2,39,40] See Ref. [65] for further details on this simulated high-efficiency case.

Figure 6 provides the results for a projected high-efficiency scenario with $R_s = 1.4$ Ω cm^2 (the experimental value for the PCBM:P3HT test cell), with $R_s = 0$ and larger R_s values. A summary of the input parameters is given in Table 2.[66] The R_s optimization in Figure 6 shows that the effects of an optimized R_s are more significant in a high-efficiency scenario, but remain modest for the test cell R_s (1.4 Ω cm^2). For $R_s = 1.4$ Ω cm^2, $\eta = 13.1\%$, and for $R_s = 0$, $\eta = 13.6\%$ – giving a 0.5% efficiency loss for an R_s of 1.4 Ω cm^2, versus 0.1% loss in the P3HT:PCBM test cell case. The efficiencies for $R_s = 0$ are calculated from Equation 3 and by applying the parameters in Tables 1 and 2. The greater sensitivity to R_s in this high-efficiency scenario is because the high-efficiency cell has a greater current density, as shown in Figure 6. Efficiency losses due to series resistance can be approximated as $\sim J_{max}{}^2 R_s$.[29] In this high-efficiency scenario, the operating current

Table 2. Derived fit parameters for a projected high-efficiency OPV cell. Note that all parameters from Equation 3 are taken to be the same as for the P3HT:PCBM test cell case other than J_o and J_L. See the main text for details.

R_s [Ω cm^2]	R_p [Ω cm^2]	n	J_o [A cm^{-2}]	J_L [A cm^{-2}]
1.4	3960	2.38	3.45×10^{-8}	0.0224

is approximately twice that of the P3HT:PCBM test cell (Figs. 3 and 6). It would be expected, therefore, that doubling this current density will increase resistive losses by approximately 4x. This is the case; efficiency losses due to the R_s increase from ~0.1% for the P3HT:PCBM test cell to ~0.5% in this high-efficiency scenario.

2.4. Effects of Cell Area on R_s

The above analysis of the P3HT:PCBM test cell shows near-optimal behavior in R_s. However, the cell area is only 0.06 cm^2—typical of laboratory-scale OPVs—and it is therefore necessary to consider how losses due to R_s change with increases in cell area. Gupta et al. studied cell area effects on power conversion efficiency, although this study primarily focuses on illumination effects from flooding the cell at its perimeter (with additional current generated at the perimeter due to scattering effects).[67] Xue et al. evaluated changes in R_s for varying experimental cell areas, but only up to 0.055 cm^2.[30]

When considering the effect of cell area on R_s, the transparent anode resistance is the dominant factor. The aluminum cathode contributes negligible resistance compared to the ITO anode, given the conductivity ratio of ~100.[68,69] Furthermore, the active layer resistance contribution does not increase with increasing cell area. Figure 7a shows this graphically for hole transport (the same analysis applies for electrons). Regardless of cell area, charge carriers travel the same distance (perpendicularly) through the active and interfacial layers, and thus, the losses due to the resistance of these layers are independent of cell area. In contrast, losses due to anode resistance increase with cell area because of the lateral flow of charge through the anode. The following simple relation is a useful way to analyze anode contributions to R_s:

$$R_s = R_{s,1} + R_{s,anode} \quad (4)$$

where $R_{s,1}$ contains the contributions from the active layer, interfacial layers, current collectors, and interconnects, and $R_{s,anode}$ is the contribution to R_s from the transparent anode. Figure 7b illustrates Equation 4 with a simple diagram, where R_s is divided into these two primary resistors in series. Note that $R_{s,1}$ is independent of cell area, whereas $R_{s,anode}$ is a function of cell area.

The relationship for this resistance contribution is determined to be:

$$R_{s,anode} = \frac{w^2}{3\sigma_{anode}h_{anode}} + \frac{ww'}{\sigma_{anode}h_{anode}} \quad (5)$$

where σ_{anode} is the anode conductivity, w is the cell active layer width, h_{anode} is the anode thickness, and w' is any additional distance between the cell perimeter and the current collector (i.e., any additional distance over which the current must flow through the ITO before reaching the current collector); a related effect is reported for inorganic photovoltaic cells.[70] For reference, we derive Equation 5 in the Supporting Information for this paper. When w' is negligible, the second term in Equation 5 goes to zero. We assume square cell geometries in determining cell area (i.e., cell area = w^2). Equation 5 enables one to calculate differences in overall R_s based on changes in cell area and anode conductivity. Applying Equations 4 and 5, we determine $R_{s,anode} = 0.5\,\Omega\,cm^2$ and $R_{s,1} = 0.9\,\Omega\,cm^2$ for our P3HT:PCBM test cell. Therefore, as cell area increases, $R_{s,anode}$ will increase according to Equation 5; however, $R_{s,1}$ will remain constant at $0.9\,\Omega\,cm^2$ regardless of cell size.

Figure 8 illustrates the factors that underlie the resistive losses arising from the anode: the anode conductivity and the cell area. For the details of the computational methodology for this analysis, see Section 5. The analysis assumes that the anode thickness remains constant.[71] Figure 8 shows that for cell areas under ~0.2 cm^2, even at relatively low anode conductivities, the efficiency loss due to anode resistance is minor. However, efficiency losses for larger cells (>0.2 cm^2) can clearly be substantial. For these larger cell dimensions, the importance of the anode conductivity increases significantly, as indicated by efficiency losses shown on the right side of the graph. When this loss analysis due to anode resistance is applied to the projected high-efficiency scenario (Section 2.3), there is even greater sensitivity to anode conductivity and cell size; Figure 9 shows these results. For low anode conductivities, efficiency losses due to R_s become significant at areas greater than ~0.02 cm^2 (compared with 0.2 cm^2 for the test cell case). The greater sensitivity of efficiency losses to cell area and anode conductivity is also evident in the tighter packing of the contours in Figure 9, compared with the results for the P3HT:PCBM test cell in Figure 8.

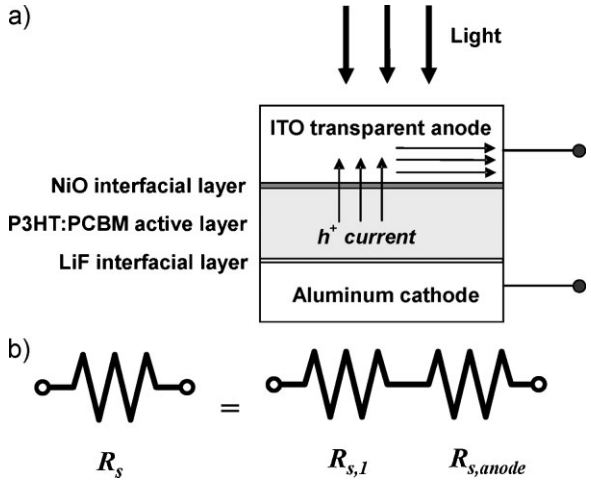

Figure 7. a) Diagram of hole current flow in a glass/ITO/NiO/P3HT:PCBM/LiF/Al BHJ OPV cell. The diagram illustrates how losses due to $R_{s,1}$ are independent of cell dimensions, whereas $R_{s,anode}$ directly depends on cell dimensions. This is because charge must flow laterally through the anode, requiring it to travel greater distances for larger cell areas, increasing losses due to the anode resistance. Note that the same analysis applies for electrons; however, since electrons flow through the aluminum cathode and the aluminum resistance is negligible compared with ITO resistance, we specifically focus on evaluating resistance losses through the ITO anode as cell area increases. b) Diagram of the two components of R_s: $R_{s,1}$ is a combination of the resistances from the active and interfacial layers, current collectors, and interconnects, and $R_{s,anode}$ is the resistance of the transparent anode. Note that $R_{s,1}$ is independent of cell dimensions, whereas $R_{s,anode}$ is a function of the cell dimensions as described by Equation 5.

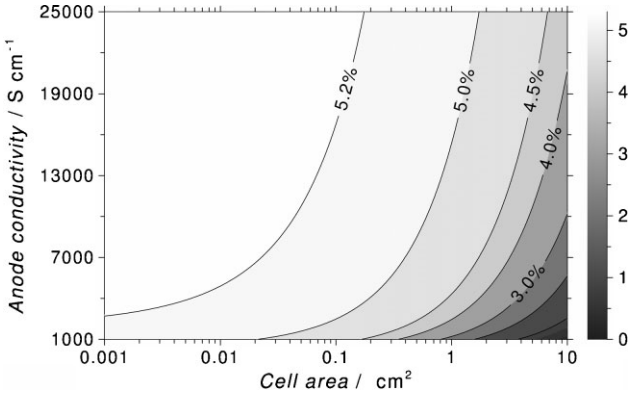

Figure 8. The effects of anode conductivity and cell area on cell power conversion efficiency for the P3HT:PCBM test cell. The measured efficiency for this cell is $\eta = 5.2\%$. The efficiency for an optimized R_s ($R_s = 0$) is calculated to be $\eta = 5.3\%$.

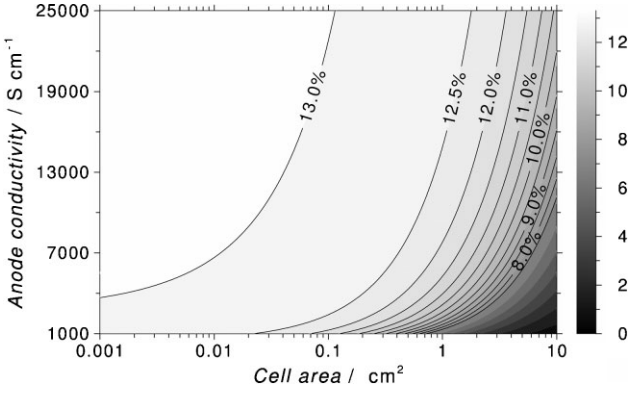

Figure 9. The effects of anode conductivity and cell area on cell power conversion efficiency in a projected high-efficiency OPV cell, as outlined in Section 2.3. The efficiency for an optimized R_s ($R_s = 0$) is calculated to be $\eta = 13.6\%$.

3. Discussion

The above analysis highlights a key result for future OPV development strategies: resistive losses for the present glass/ITO/NiO/P3HT:PCBM/LiF/Al test cell approach ideal behavior (for moderate cells areas $\leq \sim 0.1\,\text{cm}^2$). Despite the relatively low mobilities of P3HT and PCBM (time-of-flight mobilities on the order of $10^{-4}\,\text{cm}^2\,\text{V}^{-1}\,\text{s}^{-1}$),[6] they are sufficient to overcome nearly all efficiency losses arising from cell resistance. In large part, this result stems from the relatively thin active layers of OPVs[4] compared with many inorganic solar cells.[26] Note that the resistance of a material is affected by three factors – mobility, cell dimensions, and charge carrier concentration. Conductivity is calculated by:[38]

$$\sigma = en\mu \tag{6}$$

where n is the charge carrier density and μ is the carrier mobility. One can therefore calculate the resistance of a material from its conductivity (Equation 6) and the cell dimensions. The R_s contribution from the active layer has been measured experimentally, where increasing the active layer thickness (h_{AL}) gives a linear response in R_s:[72]

$$\Delta R_{s,AL} \propto \frac{\Delta h_{AL}}{\sigma_{AL}} \tag{7}$$

where $R_{s,AL}$ is the active layer contribution to R_s, and σ_{AL} is the active layer conductivity.[73] Equations 6 and 7 show that mobility is only one aspect of the active layer contribution to the cell resistance, and even for relatively low mobilities, efficiency losses due to R_s can be minimized. In comparing Equations 5 and 7, note that the h term appears in the denominator in Equation 5 and in the numerator in Equation 7. Intuitively, this is because charge carriers effectively make a right-angle turn at the electrodes, as shown in Figure 7a. Consequently, a larger h_{AL} means that charge carriers must travel further through the active layer and incur greater resistive losses, whereas a larger h_{anode} means that they have a wider (and thus, lower resistance) pathway through the anode.

The present results show that, while recent advances in P3HT:PCBM mobilities have likely led to significant efficiency enhancements via reductions in the active layer R_s contributions, *further* P3HT:PCBM active layer mobility enhancements will do little to overcome resistance losses since the performance of this particular cell is already approaching optimal behavior in R_s. For example, the annealing and self-organization experiments on P3HT:PCBM cells reported by Li et al. improved active layer hole mobilities by a factor of ~10 and reduced R_s values by a factor of ~10x (from 19.8 Ω cm^2 to 2.4 Ω cm^2).[6] Furthermore, η of the high mobility devices was ~4%, versus ~1% for the lower mobility devices. The analysis in Figure 4 demonstrates that a substantial portion of this efficiency enhancement is due to R_s reduction. However, Figure 4 also indicates that further reductions in R_s below ~1 Ω cm^2 would not significantly enhance η.

It is also important to consider potential coupling between R_s and other cell characteristics. With increasing R_s, the approach used here yields significant losses to fill factor, losses to J_{sc} when R_s is sufficiently high (~50 Ω cm^2), and no changes to V_{oc} (Figs. 3–6). By Ohm's Law, a change in voltage $\Delta V = J\Delta R$. However, when $J = 0$ (i.e., at $V = V_{oc}$), $\Delta V = 0$ as well, and therefore V_{oc} is not expected to change, as shown here. Experimentally, this result has also been observed where changes to R_s yield almost no change to V_{oc}.[6,11,30,67] Furthermore, previous studies have demonstrated no significant change to J_o, n, and R_p for varying R_s values.[6,30] One area where R_s may be significantly coupled to another parameter is J_L, due to mobility effects, thereby affecting J_{sc}. While R_s and mobility are closely linked via Equations 5, 6, and 7, mobility certainly affects other performance parameters in a solar cell beyond R_s. A large R_s is sometimes a result of low mobility materials (Equations 6 and 7), and previous reports show that low mobilities can reduce J_L if charge carrier lifetimes are less than their respective collection times.[42,54] This effect manifests itself in the J–V curve through a non-zero slope near short circuit and a reduction in J_{sc}. The effect is negligible for the present P3HT:PCBM test cell, however, as evidenced by the high quantum efficiencies and near-zero-slope J–V behavior at a zero cell voltage (Fig. 2).[14] That said, we expect that η is more sensitive to mobility than to R_s. For example, while a 10x increase in R_s has a negligible

effect on J_{sc} (see Fig. 5), the analysis reported by Schilinsky et al. indicates that a 10× decrease in electron and hole mobilities would have an appreciable deleterious effect on J_L and thus J_{sc}; see their discussion for details on this proposed mobility–J_L relationship.[42] Ultimately, however, this point simply highlights our assertion that state-of-the-art P3HT:PCBM mobilities appear to be sufficient for overcoming most losses due to resistance and charge collection. Other areas where mobility is relevant are the various conduction processes in semiconductors, such as charge injection through metal-semiconductor (Schottky) barriers[26,74] and Poole–Frenkel emission.[37,75] Furthermore, while research is ongoing in understanding exciton dissociation dynamics in OPVs,[60–64,76–78] it is possible that greater carrier mobilities could enhance exciton dissociation rates, which play a crucial role in improving overall OPV power conversion efficiencies.[2,4,63,64]

Finally, the one area where there is immediate opportunity for R_s optimization in state-of-the-art OPVs is in the anode conductivity for larger cell sizes. Figures 8 and 9 demonstrate this conclusion; for cell areas greater than ~0.2 cm^2 and ~0.02 cm^2, respectively, anode conductivity becomes increasingly important in reducing losses due to cell resistance. Alternative transparent anode materials have received significant attention in recent years,[79–83] and transparent conducting oxides (TCOs) with exceptionally high conductivities of over 17,000 S cm^{-1} have been reported.[68,84] These high conductivity TCOs are approaching the intrinsic limit of ~25,000 S cm^{-1} proposed by Bellingham, Phillips, and Adkins.[85] Figures 8 and 9 show the cell sizes at which these high conductivities are important in OPVs: if an OPV manufacturer sought to reduce costs through increasing current collector spacing (i.e., larger cell areas), then these high conductivity TCO materials would become increasingly important.

4. Conclusions

We show here that efficiency losses arising from cell resistance (R_s) in optimized glass/ITO/NiO/P3HT:PCBM/LiF/Al BHJ solar cells are minor: removing all losses due to cell resistance is estimated to lead to an efficiency improvement of only ~0.1% (from $\eta = 5.2\%$ to $\eta = 5.3\%$) in our test cell. Resistive losses become significant only for relatively large cell dimensions, where anode conductivity is an important contributor to these losses. For a projected future high-efficiency OPV scenario, losses due to R_s become more significant, but remain modest for our test cell area of 0.06 cm^2 (increasing to 0.5% vs. 0.1% for the present cells). Furthermore, there is greater sensitivity to cell size for cell areas greater than ~0.02 cm^2 in projected high-efficiency OPVs. Therefore, for future high-efficiency OPVs, a key component is likely to be higher conductivity anode materials, which would substantially reduce R_s losses for modest cell sizes and are the only means to impact R_s significantly in these cells (assuming an active layer contribution to R_s comparable to P3HT:PCBM). The resistance of the P3HT:PCBM active layer, on the other hand, is nearly optimal; with all other factors remaining equal, further mobility improvements in these active layer materials should have minor effects in reducing resistance losses. Further studies will be necessary to articulate more completely how high mobility OPV materials affect other types of losses (e.g., charge carrier recombination or exciton dissociation losses).

It is evident that OPVs will not advance beyond the 10% efficiency threshold without new donor and acceptor materials that increase V_{oc} and absorb larger portions of the solar spectrum for enhanced J_{sc} values. Developing modeling and analytical approaches is crucial to understanding the requirements for these new materials, particularly regarding the question of required $LUMO_D$-$LUMO_A$ separation. For future OPV research efforts, resistance losses are therefore always important considerations, but new active layer materials are critical to overcoming V_{oc} and J_{sc} losses incurred in today's best OPV systems.

5. Computational Methodology

To determine the dark fit parameters, a least-squares fit was employed to solve numerically for the parameters, applying Equation 3 without the J_L term (as there is no photocurrent in the dark). Using these fit parameters, it was then possible to apply Equation 3 in simulating J–V data based on changes in R_s, equating the experimental J_{sc} to J_L according to Ref. [28]. Waldauf et al. have shown how R_p varies with light intensity (see Ref. [49]). To address this dependence, the same method used for the dark data was applied to the light data and an R_p of 3960 Ω cm^2 for the light J–V curve was determined; the dark R_p, on the other hand, was determined to be 41,400 Ω cm^2. While the difference between the light and dark R_p values is large, this difference has only a slight effect on the behavior of the simulated curves for this data set, and both light and dark R_p values therefore give excellent simulations of the cell response. To generate Figures 4 and 5, which show the effects of R_s on J_{sc}, fill factor, and η, Equation 3 was solved numerically to generate new J–V data sets for successive changes in R_s and to calculate J_{sc}, fill factor, and η. To calculate losses due to anode resistance (Figs. 8 and 9), Equation 3 was solved numerically to generate new J–V data sets at each point and to determine new maximum η values. This process requires first extracting the P3HT:PCBM test cell anode contribution to R_s to calculate a "zero loss" case and then determining the new anode R_s contribution based upon modeled anode conductivity and cell area.

Acknowledgements

We thank BP Solar, the U.S. Office of Naval Research, and U.S. DOE (DE-FG02-08ER46536/A000) for support of this research. We thank J. Liu, M. Irwin, and A. Hains for useful discussions. Supporting Information is available online from Wiley InterScience or from the authors.

Received: June 23, 2009
Published online: October 8, 2009

[1] C. W. Tang, *Appl. Phys. Lett.* **1986**, *48*, 183.
[2] K. M. Coakley, M. D. McGehee, *Chem. Mater.* **2004**, *16*, 4533.
[3] S. Gunes, H. Neugebauer, N. S. Sariciftci, *Chem. Rev.* **2007**, *107*, 1324.
[4] G. Dennler, M. C. Scharber, C. J. Brabec, *Adv. Mater.* **2009**, *21*, 1.
[5] B. Kippelen, J.-L. Brédas, *Energy Environ. Sci.* **2009**, *2*, 251.
[6] G. Li, V. Shrotriya, J. S. Huang, Y. Yao, T. Moriarty, K. Emery, Y. Yang, *Nat. Mater.* **2005**, *4*, 864.
[7] C. J. Brabec, *Sol. Energy Mater. Sol. Cells* **2004**, *83*, 273.
[8] M. A. Green, K. Emery, Y. Hisikawa, W. Warta, *Prog. Photovoltaics* **2007**, *15*, 425.
[9] NREL: Thin Films Partnership Program – News Feature, http://www.nrel.gov/pv/thin_film/cfm/news.cfm/ID=5544/report=news (accessed September 5, 2009).
[10] G. Yu, J. Gao, J. C. Hummelen, F. Wudl, A. J. Heeger, *Science* **1995**, *270*, 1789.
[11] W. L. Ma, C. Y. Yang, X. Gong, K. Lee, A. J. Heeger, *Adv. Funct. Mater.* **2005**, *15*, 10.

[12] J. Peet, J. Y. Kim, N. E. Coates, W. L. Ma, D. Moses, A. J. Heeger, G. C. Bazan, *Nat. Mater.* **2007**, *6*, 497.
[13] J. Y. Kim, K. Lee, N. E. Coates, D. Moses, T. Q. Nguyen, M. Dante, A. J. Heeger, *Science* **2007**, *317*, 222.
[14] M. D. Irwin, B. Buchholz, A. W. Hains, R. P. H. Chang, T. J. Marks, *Proc. Natl. Acad. Sci. USA* **2008**, *105*, 2783.
[15] S. H. Park, A. Roy, S. Beaupre, S. Cho, N. Coates, J. S. Moon, D. Moses, M. Leclerc, K. Lee, A. J. Heeger, *Nat. Photonics* **2009**, *3*, 297.
[16] R. W. Birkmire, E. Eser, *Annu. Rev. Mater. Sci.* **1997**, *27*, 625.
[17] N. S. Sariciftci, D. Braun, C. Zhang, V. I. Srdanov, A. J. Heeger, G. Stucky, F. Wudl, *Appl. Phys. Lett.* **1993**, *62*, 585.
[18] P. Peumans, A. Yakimov, S. R. Forrest, *J. Appl. Phys.* **2003**, *93*, 3693.
[19] F. Padinger, R. S. Rittberger, N. S. Sariciftci, *Adv. Funct. Mater.* **2003**, *13*, 1.
[20] R. Kroon, M. Lenes, J. C. Hummelen, P. W. M. Blom, B. De Boer, *Polym. Rev.* **2008**, *48*, 531.
[21] A. B. Tamayo, X. Dang, B. Walker, J. Seo, T. Kent, T. Nguyen, *Appl. Phys. Lett.* **2009**, *94*, 103301.
[22] R. B. Ross, C. M. Cardona, D. M. Guldi, S. G. Sankaranarayanan, M. O. Reese, N. Kopidakis, J. Peet, B. Walker, G. C. Bazan, E. Van Keuren, B. C. Holloway, M. Drees, *Nat. Mater.* **2009**, *8*, 208.
[23] W. U. Huynh, J. J. Dittmer, A. P. Alivisatos, *Science* **2002**, *295*, 2425.
[24] K. M. Coakley, M. D. McGehee, *Appl. Phys. Lett.* **2003**, *83*, 3380.
[25] A. W. Hains, T. J. Marks, *Appl. Phys. Lett.* **2008**, *92*, 023504.
[26] S. M. Sze, *Physics of Semiconductor Devices*, Wiley-Interscience, New York **1981**.
[27] M. A. Green, *Solar Cells: Operating Principles, Technology, and System Applications*, Prentice-Hall, Englewood Cliffs, NJ, USA **1982**.
[28] J. Nelson, *The Physics of Solar Cells*, Imperial College Press, London, England **2003**.
[29] A. L. Fahrenbruch, R. H. Bube, *Fundamentals of Solar Cells*, Academic, New York, USA **1983**.
[30] J. G. Xue, S. Uchida, B. P. Rand, S. R. Forrest, *Appl. Phys. Lett.* **2004**, *84*, 3013.
[31] K. Nakayama, Y. Matsui, M. Yokoyama, *Jpn. J. Appl. Phys. Part 1* **2005**, *44*, 633.
[32] F. Yang, M. Shtein, S. R. Forrest, *Nat. Mater.* **2005**, *4*, 37.
[33] H. Hoppe, M. Niggemann, C. Winder, J. Kraut, R. Hiesgen, A. Hinsch, D. Meissner, N. S. Sariciftci, *Adv. Funct. Mater.* **2004**, *14*, 1005.
[34] Y. Kim, S. Cook, S. M. Tuladhar, S. A. Choulis, J. Nelson, J. R. Durrant, D. D. C. Bradley, M. Giles, I. McCulloch, C. S. Ha, M. Ree, *Nat. Mater.* **2006**, *5*, 197.
[35] D. Mihailetchi, H. X. Xie, B. de Boer, L. J. A. Koster, P. W. M. Blom, *Adv. Funct. Mater.* **2006**, *16*, 699.
[36] R. McNeill, J. J. M. Halls, R. Wilson, G. L. Whiting, S. Berkebile, M. G. Ramsey, R. H. Friend, N. C. Greenham, *Adv. Funct. Mater.* **2008**, *18*, 2309.
[37] M. Pope, C. E. Swenberg, *Electronic Processes in Organic Crystals*, Oxford University Press, Oxford, England **1982**.
[38] N. W. Ashcroft, N. D. Mermin, *Solid State Physics*, Holt, Rinehart and Winston, New York, USA **1976**, pp. 1–28.
[39] M. C. Scharber, D. Wuhlbacher, M. Koppe, P. Denk, C. Waldauf, A. J. Heeger, C. L. Brabec, *Adv. Mater.* **2006**, *18*, 789.
[40] L. J. A. Koster, V. D. Mihailetchi, P. W. M. Blom, *Appl. Phys. Lett.* **2006**, *88*, 3.
[41] P. Schilinsky, C. Waldauf, C. J. Brabec, *Adv. Funct. Mater.* **2006**, *16*, 13.
[42] P. Schilinsky, C. Waldauf, J. Hauch, C. J. Brabec, *J. Appl. Phys.* **2004**, *95*, 2816.
[43] W. U. Huynh, J. J. Dittmer, N. Teclemariam, D. J. Milliron, A. P. Alivisatos, K. W. J. Barnham, *Phys. Rev. B* **2003**, *67*, 12.
[44] S. Yoo, B. Domercq, B. Kippelen, *J. Appl. Phys.* **2005**, *97*, 9.
[45] W. Shockley, *Bell Syst. Tech. J.* **1949**, *28*, 7.
[46] C. T. Sah, R. N. Noyce, W. Shockley, *Proc. IRE* **1957**, *45*, 1228.
[47] W. Shockley, W. T. Read, *Phys. Rev.* **1952**, *87*, 835.
[48] R. N. Hall, *Phys. Rev.* **1951**, *83*, 228.
[49] C. Waldauff, P. Schilinsky, J. Hauch, C. J. Brabec, *Thin Solid Films* **2004**, *451*, 503.
[50] L. J. A. Koster, E. C. P. Smits, V. D. Mihailetchi, P. W. M. Blom, *Phys. Rev. B* **2005**, *72*, 8.
[51] Z. E. Ooi, R. Jin, J. Huang, Y. F. Loo, A. Sellingera, J. C. deMello, *J. Mater. Chem.* **2008**, *18*, 1644.
[52] P. W. M. Blom, V. D. Mihailetchi, L. J. A. Koster, D. E. Markov, *Adv. Mater.* **2008**, *20*, 12.
[53] R. A. Marsh, C. R. McNeill, A. Abrusci, A. R. Campbell, R. H. Friend, *Nano Lett.* **2008**, *8*, 1393.
[54] I. Riedel, V. Dyakonov, *Phys. Status Solidi A* **2004**, *201*, 1332.
[55] F. Shirland, *Adv. Energy Convers.* **1966**, *6*, 201.
[56] B. A. Gregg, S. Chen, R. A. Cormier, *Chem. Mater.* **2004**, *16*, 4586.
[57] A. Dhanabalan, J. K. J. van Duren, P. A. van Hal, J. L. J. van Dongen, R. A. J. Janssen, *Adv. Funct. Mater.* **2001**, *11*, 255.
[58] B. C. Thompson, J. M. J. Frechet, *Angew. Chem. Int. Ed.* **2008**, *47*, 58.
[59] F. B. Kooistra, J. Knol, F. Kastenberg, L. M. Popescu, W. J. H. Verhees, J. M. Kroon, J. C. Hummelen, *Org. Lett.* **2007**, *9*, 551.
[60] J.-L. Brédas, D. Beljonne, V. Coropceanu, J. Cornil, *Chem. Rev.* **2004**, *104*, 11.
[61] M. Mandoc, W. Veurman, L. J. A. Koster, B. de Boer, P. W. M. Blom, *Adv. Funct. Mater.* **2007**, *17*, 2167.
[62] T. M. Clarke, A. M. Ballantyne, J. Nelson, D. D. C. Bradley, J. R. Durrant, *Adv. Funct. Mater.* **2008**, *18*, 7.
[63] H. Ohkita, S. Cook, Y. Astuti, W. Duffy, S. Tierney, W. Zhang, M. Heeney, I. McCulloch, J. Nelson, D. D. C. Bradley, J. R. Durrant, *J. Am. Chem. Soc.* **2008**, *130*, 3030.
[64] D. Veldman, S. C. J. Meskers, R. A. J. Janssen, *Adv. Funct. Mater.* **2009**, *19*, 1.
[65] J. D. Servaites, T. J. Marks, M. A. Ratner, *Appl. Phys. Lett.*, in press.
[66] Note that J_L and J_o are the only parameters from Equation 3 that change between the experimental (5.2%) case and the high-efficiency case. The larger value for J_L is simply due to the larger J_{sc} in the high-efficiency scenario. While the theory underlying J_o is well-established for *p–n* junction solar cells (see Refs. [45,46]), it is not well-developed for BHJ OPVs, and studies are still in progress. Discussion of the parameter can be found in Ref. [41].
[67] D. Gupta, M. Bag, K. S. Narayan, *Appl. Phys. Lett.* **2008**, *93*, 163301.
[68] Y. Yang, S. Jin, J. E. Medvedeva, J. R. Ireland, A. W. Metz, J. Ni, M. C. Hersam, A. J. Freeman, T. J. Marks, *J. Am. Chem. Soc.* **2005**, *127*, 8796.
[69] *Handbook of Chemistry and Physics* (Ed: R. C. Weast), 65th ed, CRC Press, Boca Raton, FL, USA **1984**.
[70] N. C. Wyeth, *Solid-State Electron.* **1977**, *20*, 629.
[71] Note that while increasing the anode thickness will decrease the anode contribution to R_s, as shown in Equation 5, there is a counter effect in that the optical transmission of the anode is reduced with increasing thicknesses. Therefore, the best way to address the anode contribution to R_s is to use higher conductivity materials.
[72] T. Aernouts, W. Geens, J. Poortmans, P. Heremans, S. Borghs, R. Mertens, *Thin Solid Films* **2002**, *403–404*, 297.
[73] Note that charge generation profiles can also affect how an increase in active layer thickness affects R_s. For example, if more electrons form near the transparent anode, they have a larger distance to travel before arriving at the aluminum cathode (thus affecting resistance losses), compared with forming near the cathode. This charge generation profile will be system-specific; see Ref. [4] for BHJ OPV profiles.
[74] S. M. Sze, C. R. Crowell, D. Kahng, *J. Appl. Phys.* **1964**, *35*, 2534.
[75] J. Frenkel, *Phys. Rev.* **1938**, *54*, 8.
[76] C. L. Braun, *J. Chem. Phys.* **1984**, *80*, 4157.
[77] T. Offermans, S. C. J. Meskers, R. A. J. Janssen, *Chem. Phys.* **2005**, *308*, 125.
[78] C. Deibel, A. Wagenpfahl, V. Dyakonov, *Phys. Status Solidi RRL* **2008**, *2*, 175.
[79] R. G. Gordon, *MRS Bull.* **2000**, *25*, 52.
[80] D. S. Ginley, C. Bright, *MRS Bull.* **2000**, *25*, 15.
[81] J. F. Wager, *Science* **2003**, *300*, 1245.
[82] H. Hosono, *Thin Solid Films* **2007**, *515*, 6000.
[83] E. Fortunato, D. Ginley, H. Hosono, D. C. Paine, *MRS Bull.* **2007**, *32*, 3.
[84] A. Wang, J. R. Babcock, N. L. Edleman, A. W. Metz, M. A. Lane, R. Asahi, V. P. Dravid, C. R. Kannewurf, A. J. Freeman, T. J. Marks, *Proc. Natl. Acad. Sci. USA* **2001**, *98*, 7113.
[85] J. R. Bellingham, W. A. Phillips, C. J. Adkins, *J. Mater. Sci. Lett.* **1992**, *11*, 263.